Inorganic Chemistry
Article

Inorg. Chem. **2009**, *48*, 6303–6313 **6303**
DOI: 10.1021/ic900579s

Substituent Effect on Oxygen Atom Transfer Reactivity from Oxomolybdenum Centers: Synthesis, Structure, Electrochemistry, and Mechanism

Partha Basu,* Victor N. Nemykin,† and Raghvendra S. Sengar

Department of Chemistry and Biochemistry, Duquesne University, Pittsburgh, Pennsylvania 15282.
† Current address: Department of Chemistry, University of Minnesota-Duluth, Duluth, MN

Received March 24, 2009

Dioxo molybdenum complexes of general formula $Tp^*MoO_2(S\text{-}p\text{-}RC_6H_4)$ (**1**), where Tp* = hydrotris(3,5-dimethyl-1-pyrazolyl)borate and R = OMe, Me, SMe, NHCOMe, H, Cl, CF_3, NO_2, were reacted with trimethyl phosphine (PMe_3) to convert into complexes of general formula $Tp^*MoO(S\text{-}p\text{-}RC_6H_4)(OPMe_3)$ (**2**) (where R = OMe, Me, SMe, H, Cl, and CF_3). These complexes were isolated and characterized by NMR, IR, UV/vis, and single crystal X-ray crystallography. Electronic and NMR spectra, as well as redox potentials vary as a function of substituent on the thiophenolato ligand. When viewed entirety of the oxygen atom transfer (OAT) reactivity, the reaction of $Tp^*MoO_2(S\text{-}p\text{-}RC_6H_4)$ with PMe_3 shows a biphasic behavior, indicating the formation of at least one intermediate. The kinetics of the both steps, that is, the formation of the phosphoryl intermediate and the formation of the solvent coordinated species have been investigated by UV−vis spectroscopy. The first step follows a second order process, first order with respect to both the complex and PMe_3, and the overall second order rate constants at 25 °C range from 98.2 ($\pm$0.01) $\times$ 10^{-2} M^{-1} s^{-1} (for R = OMe) to 223.0 ($\pm$0.20) $\times$ 10^{-2} M^{-1} s^{-1} (for R = CF_3); activation parameters were in the ranges $\Delta H^{\ddagger}$ = 49.3 ($\pm$4.1) kJ·mol^{-1} (for R = OMe) to 34.0 ($\pm$7.5) kJ·mol^{-1} (for R = CF_3), $\Delta S^{\ddagger}$ = −154.0 ($\pm$14.2) J·mol^{-1}·K^{-1} (for R = OMe) to −184.3 ($\pm$26.1) J·mol^{-1} K^{-1} (for R = CF_3), and $\Delta G^{\ddagger}$ = 95.0 kJ·mol^{-1} (for R = OMe) to 88.7 kJ·mol^{-1} (for R = CF_3). Formation of the acetonitrile complex from the phosphoryl complex follows a first order process with respect to the complex. The first order rate constants at 25 °C range from 3.60 ($\pm$0.01) $\times$ 10^{-4} sec^{-1} (for R = OMe) to 6.32 ($\pm$0.11) $\times$ 10^{-4} sec^{-1} (for R = CF_3), and the enthalpy of activation and entropy of activation show variation; $\Delta H^{\ddagger}$ = 62.5 ($\pm$2.2) to 67.8 ($\pm$1.0) kJ·mol^{-1}, $\Delta S^{\ddagger}$ = −82.5 ($\pm$3.3) to −101.3 ($\pm$7.5) J·mol^{-1}·K^{-1}, but the free energy of activation remains constant $\Delta G^{\ddagger} \sim$ 92 ($\pm$1) kJ·mol^{-1}. Large entropies of activation associated with both steps are consistent with associative transition states. The comparable magnitude of the activation energy of the two steps underscores the difficulty in identifying the rate-limiting step in the overall OAT reaction. The first step, however, is more sensitive toward the substituent effects than the second step. Therefore, a change in the substituent can play an important role in deciding the rate-limiting step involved in a two-step OAT reaction.

Introduction

In nature, pterin-containing mononuclear molybdenum enzymes are widely distributed through all forms of life.[1] These enzymes catalyze key metabolic processes and are active participants in the global biogeochemical cycles of elements such as carbon, nitrogen, sulfur, arsenic, and selenium. In general, enzymes such as sulfite oxidase, dimethyl sulfoxide reductase, and nitrate reductase catalyze net oxygen atom transfer (OAT) reactions at the mononuclear oxomolybdenum active centers.[1] Although the details of the mechanism may vary, non-molybdenum enzymes such as cytochrome P450 are also thought to proceed via similar reactions. Catalytic OAT reactions are also important in industrial processes such as the epoxidation of olefin.[2−4]

The overall OAT reaction is also a defining reaction in synthetic oxo-molybdenum chemistry.[5−11] OAT reactions are a subset of atom transfer reactions, and as such these reactions have been reported for other transition metal, for

*To whom correspondence should be addressed. E-mail: basu@duq.edu.

(1) McMaster, J.; Garner, C. D.; Stiefel, E. I. Molybdenum Enzymes. In *Biological Inorganic Chemistry, Structure and Reactivity*; Bertini, I., Gary, H. B., Stiefel, E. I., Valentine, J. S., Eds.; University Science Books: Sausalito, CA, 2007.

(2) Thiel, W. R.; Barz, M.; Glas, H.; Pleier, A.-K. *Peroxide Chem.* **2000**, 433.
(3) Nugent, W. A.; RajanBabu, T. V.; Burk, M. J. *Science* **1993**, *259*, 479.
(4) Sharpless, K. B.; Townsend, J. M.; Williams, D. R. *J. Am. Chem. Soc.* **1972**, *94*, 295.
(5) Holm, R. H. *Chem. Rev.* **1987**, *87*, 1401.
(6) Holm, R. H. *Coord. Chem. Rev.* **1990**, *100*, 183.
(7) Arzoumanian, H. *Coord. Chem. Rev.* **1998**, *178−180*, 191.
(8) Enemark, J. H.; Cooney, J. J. A.; Wang, J.-J.; Holm, R. H. *Chem. Rev.* **2004**, *104*, 1175.
(9) Du, G.; Abu-Omar, M. M. *Curr. Org. Chem.* **2008**, *12*, 1185.
(10) Lyashenko, G.; Saischek, G.; Pal, A.; Herbst-Irmer, R.; Moesch-Zanetti, N. C. *Chem. Commun.* **2007**, 701.
(11) Tran, B. L.; Carrano, C. J. *Inorg. Chem.* **2007**, *46*, 5429.

Published on Web 06/01/2009

example, rhenium, vanadium, and tungsten complexes.[12−17] In most cases, OAT reactions involve higher-valent metal centers, and the reaction proceeds with concomitant reduction of the donor center by two electrons as shown in eq 1. OAT reactions involving oxo-molybdenum complexes

$$MO^{n+} + X \rightarrow M^{(n-2)+} + XO \quad (1)$$

containing dithiocarbamate,[18,19] ene-dithiolate,[20−31] and hydrotris(pyrazolyl)borate[32−34] as well as other ligands[10,35,36] have been reported. While a variety of biological substrates have been used in investigating such reactions in model systems, tertiary phosphines (PR_3) have become the reagents of choice because of their high solubility in organic solvents and the ability to tune their reactivity through substitution at phosphorus. For a number of years we have been engaged in delineating the details of OAT reactivity using tertiary phosphines as model substrates.[32,37−41]

Traditionally, OAT reactions from $Mo^{VI}O_2$ centers to PR_3 are thought to proceed via nucleophilic attack by the phosphine on an empty Mo=O π^* orbital.[5,42] In these reactions, the existence of a single transition state was supported by experimental data. More recent theoretical and experimental investigation indicated that the overall reactions proceed via the formation of a phosphine oxide-coordinated intermediate.[32,43,44] The phosphoryl intermediate of general formula [Tp*MoO(OPR_3)X], in which Tp* = hydrotris(3,5-dimethylpyrazol-1-yl)borate; X = SPh, OPh, Br, and Cl, and [Tp^{iPr}-MoO(OPR_3)X] (Tp^{iPr} = hydrotris(3-isopropylpyrazol-1-yl) borate; X = Cl, substituted phenolate, or alkyl thiolate) has been detected, isolated, and characterized.[37,38,40,41,45] Mechanistically, the first step involves the formation of the phosphoryl intermediate, and in the second step the phosphine oxide is solvolyzed. In this report we present complexes with Mo^{VI}—S unit which is also present in sulfite oxidase (SO), where the sulfur donor comes from a cysteine.[46] Herein we report complexes with a Mo−S(thiophenol) unit which allows systematic perturbation at the thiophenol group providing a vehicle for a detailed understanding of the electronic effect on reactivity. Thus, syntheses and spectroscopic characterization of Tp*MoO_2(S-*p*-RC_6H_4) (where R = OMe, Me, SMe, NHCOMe, H, Cl, CF_3, and NO_2), and Tp*MoO(S-*p*-RC_6H_4)($OPMe_3$) (where R = OMe, Me, SMe, H, Cl, and CF_3) (Chart 1) are reported here. In addition, we report the structures, redox chemistry, and reactivity of both the dioxo-Mo(VI) and the phosphoryl Mo(IV) complexes. The complex with an unsubstituted thiophenol has recently been reported,[41] which is used here for completeness.

Experimental Section

Spectroscopy and Electrochemistry. Room temperature ^1H, ^{13}C, and ^{31}P NMR spectra were recorded using a Bruker ACP-300 spectrometer at 300.133 MHz, 75.469 MHz, and 121.496 MHz frequencies, respectively. Deuterated solvents were obtained from Cambridge Isotope Laboratory and used as received. Infrared spectra were recorded on a Perkin-Elmer FT-IR 1760X spectrometer on NaCl plates or in KBr pellets. Mass spectra were collected on a Micromass ZMD mass spectrometer using both negative and positive ionization mode. Acetonitrile solutions of the samples were injected via a syringe pump with a flow rate of 0.1−0.2 mL/min. Electronic spectra of complexes were recorded in Cary 3 and Cary 14 spectrophotometers. Cyclic voltammograms (CVs) of all the dioxo-Mo^{VI} and monooxo-Mo^{IV} complexes were recorded in a Bioanalytical systems (BAS) model CV-50W using a standard three electrode system consisting of Pt-disk working and reference electrodes and a Pt-wire auxiliary electrode in dry and degassed acetonitrile, containing 0.1 M Bu_4NClO_4 as supporting electrolyte. At the end of each measurement the potentials were internally calibrated with Fc^+/Fc couple, and presented with respect to Fc^+/Fc couple at the same scan rate (100 mV/s). Electrochemical measurements of monooxo-Mo^{IV} phosphoryl complexes were completed in less than 2 min, and up to 7% of the phosphoryl ligand exchanged during this time. The first scan was recorded at a rate of 100 mV/s within 30 s of dissolution of the complex in acetonitrile during which ~1% ligand exchanged.

X-ray Crystallography. Brown crystals of dioxo-Mo^{VI} complexes **1a**, **1b**, **1f**, and **1h** or bright green crystals of **2a**, **2f**, and **2g** were obtained by vapor diffusion of hexane into the benzene or toluene solution of the complex. Crystals of complex **1d** were obtained by slow diffusion of toluene into the acetonitrile solutions of the complex. X-ray quality single crystals were mounted on glass fibers and coated with the epoxy resin, the intensities were recorded on a Rigaku AFC-7R four-circle X-ray diffractometer using graphite-monochromatized Mo-K_α

(12) Woo, L. K. *Chem. Rev.* **1993**, *93*, 1125.
(13) Espenson, J. H. *Adv. Inorg. Chem.* **2003**, *54*, 157.
(14) Espenson, J. H. *Coord. Chem. Rev.* **2005**, *249*, 329.
(15) Gable, K. P. *Adv. Organomet. Chem.* **1997**, *41*, 127.
(16) Gable, K. P.; Brown, E. C. *J. Am. Chem. Soc.* **2003**, *125*, 11018.
(17) Mayer, J. M. *Chemtracts: Inorg. Chem.* **1992**, *4*, 380.
(18) Barral, R.; Bocard, C.; Seree de Roch, I.; Sajus, L. *Tetrahedron Lett.* **1972**, 1693.
(19) Reynolds, M. S.; Berg, J. M.; Holm, R. H. *Inorg. Chem.* **1984**, *23*, 3057.
(20) Majumdar, A.; Pal, K.; Sarkar, S. *J. Am. Chem. Soc.* **2006**, *128*, 4196.
(21) Majumdar, A.; Pal, K.; Sarkar, S. *Inorg. Chem.* **2008**, *47*, 3393.
(22) Das, S. K.; Chaudhury, P. K.; Biswas, D.; Sarkar, S. *J. Am. Chem. Soc.* **1994**, *116*, 9061.
(23) Oku, H.; Ueyama, N.; Kondo, M.; Nakamura, A. *Inorg. Chem.* **1994**, *33*, 209.
(24) Jiang, J. F.; Holm, R. H. *Inorg. Chem.* **2005**, *44*, 1068.
(25) Sung, K. M.; Holm, R. H. *J. Am. Chem. Soc.* **2002**, *124*, 4312.
(26) Sung, K. M.; Holm, R. H. *J. Am. Chem. Soc.* **2001**, *123*, 1931.
(27) Lim, B. S.; Holm, R. H. *J. Am. Chem. Soc.* **2001**, *123*, 1920.
(28) Tano, H.; Tajima, R.; Miyake, H.; Itoh, S.; Sugimoto, H. *Inorg. Chem.* **2008**, *47*, 7465.
(29) Sugimoto, H.; Tarumizu, M.; Tanaka, K.; Miyake, H.; Tsukube, H. *Dalton Trans.* **2005**, 3558.
(30) Sugimoto, H.; Tarumizu, M.; Miyake, H.; Tsukube, H. *Eur. J. Inorg. Chem.* **2006**, 4494.
(31) Wang, J.-J.; Kryatova, O. P.; Rybak-Akimova, E. V.; Holm, R. H. *Inorg. Chem.* **2004**, *43*, 8092.
(32) Kail, B. W.; Perez, L. M.; Zaric, S.; Millar, A. J.; Young, C. G.; Hall, M. B.; Basu, P. *Chem.—Eur. J.* **2006**, *12*, 7501.
(33) Eagle, A. A.; Tiekink, E. R. T.; Young, C. G. *Inorg. Chem.* **1997**, *36*, 6315.
(34) Laughlin, L. J.; Young, C. G. *Inorg. Chem.* **1996**, *35*, 1050.
(35) Heinze, K.; Marano, G.; Fischer, A. *J. Inorg. Biochem.* **2008**, *102*, 1199.
(36) Hammes, B. S.; Chohan, B. S.; Hoffman, J. T.; Einwachter, S.; Carrano, C. J. *Inorg. Chem.* **2004**, *43*, 7800.
(37) Smith, P. D.; Millar, A. J.; Young, C. G.; Ghosh, A.; Basu, P. *J. Am. Chem. Soc.* **2000**, *122*, 9298.
(38) Nemykin, V. N.; Laskin, J.; Basu, P. *J. Am. Chem. Soc.* **2004**, *126*, 8604.
(39) Nemykin, V. N.; Davie, S. R.; Mondal, S.; Rubie, N.; Kirk, M. L.; Somogyi, A.; Basu, P. *J. Am. Chem. Soc.* **2002**, *124*, 756.
(40) Millar, A. J.; Doonan, C. J.; Smith, P. D.; Nemykin, V. N.; Basu, P.; Young, C. G. *Chem.—Eur. J.* **2005**, *11*, 3255.
(41) Sengar, R. S.; Nemykin, V. N.; Basu, P. *J. Inorg. Biochem.* **2008**, *102*, 748.
(42) Taube, H. *ACS Symp. Ser.* **1982**, *198*, 151.
(43) Zaric, S.; Hall, M. B. *NATO ASI Ser.* **1997**, *41*, 255.
(44) Pietsch, M. A.; Hall, M. B. *Inorg. Chem.* **1996**, *35*, 1273.
(45) Nemykin, V. N.; Basu, P. *Inorg. Chem.* **2005**, *44*, 7494.
(46) Kisker, C.; Schindelin, H.; Pacheco, A.; Wehbi, W. A.; Garrett, R. M.; Rajagopalan, K. V.; Enemark, J. H.; Rees, D. C. *Cell* **1997**, *91*, 973.

Chart 1

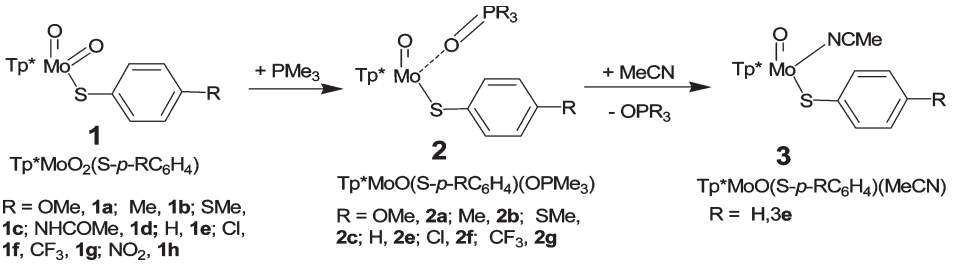

radiation (λ = 0.71069 Å) at room temperature using $\omega-2\theta$ scan. The structures were solved by Patterson method using teXsan crystallographic software package;[47] then they were refined using the Crystal for Windows package.[48] The solvent benzene molecules in the phosphoryl complexes (**2a** and **2f**) were found to be disordered and were modeled as planar with restrained C−C distance as 1.39 (±0.02) Å and C−C−C angle as 120.0 (±0.02)°.

General Procedure of the Synthesis of Dioxo-Mo^{VI} Complexes Tp*MoO$_2$(S-p-RC$_6$H$_4$) R = OMe, Me, SMe, NHCOMe, H, Cl, CF$_3$, NO$_2$. All reactions were performed anaerobically using anhydrous solvents. A mixture of suitable *para*-substituted benzenethiol and triethylamine in CH_2Cl_2 was added into a suspension of Tp*MoO$_2$Cl in CH_2Cl_2 at the room temperature. The yellow reaction mixture turned to brown over a period of 1−6 h depending on the benzenethiol used. The progress of reaction was monitored by thin layer chromatography. After completion of the reaction, the solvent was evaporated, and the brown residue was chromatographed on silica gel using toluene (or a mixture of toluene and acetonitrile) as an eluent.

General Procedure of the Synthesis of Monooxo-Mo^{IV} Phosphoryl Complexes, Tp*MoO(S-p-RC$_6$H$_4$)(OPMe$_3$) R = OMe, Me, SMe, H, Cl, CF$_3$. All the reaction and workup were performed under anaerobic conditions using anhydrous solvents. The dioxo-Mo^{VI} complex of a particular thiol was dissolved in dry benzene (or toluene), to which 4-fold excess of PMe_3 was added whereby the color of the mixture changed from dark brown to green. Partial evaporation of solvent followed by addition of hexane yielded a green precipitate, which was filtered and washed with hexane several times yielding the target compound.

Kinetic Measurements. Kinetic measurements were performed anaerobically in acetonitrile solutions. Progress of the reaction was monitored spectrophotometrically at a suitable wavelength. All kinetic data were analyzed using the Origin 6.1 software packages. The activation parameters were determined using Arrhenius and Eyring relations using variable temperature (5−30 °C) kinetic data. For the second order reactions the rate constants were normalized for concentration.

Kinetics of Formation of the Phosphoryl Intermediate, Tp*MoO(S-p-RC$_6$H$_4$)(OPMe$_3$). Reactions of dioxo-Mo^{VI} complexes with PMe_3 followed a second order process, first order both in complex and in phosphine. The reactions were followed under pseudo first order conditions with the concentration of the dioxo-Mo^{VI} complex 3−5 mM, and an excess of PMe_3. The solutions were equilibrated before mixing, and the reactions were monitored within 10 s of mixing. The formations of the intermediate complexes were monitored by single wavelength assays at an appropriate wavelength between 393 and 398 nm. The wavelengths were selected based on the location of the isosbestic point for solvation of the phosphoryl intermediate.

Kinetics of Solvolysis of Tp*MoO(S-p-RC$_6$H$_4$)(OPMe$_3$). The solvolysis reactions in acetonitrile were monitored at ~ 414 nm. For a typical experiment, ~2−3 mg of the phosphoryl complex was dissolved in 1.5 mL of pre-equilibrated acetonitrile in a cuvette and placed in an isothermal cell holder. Temperature was equilibrated for 3−4 min before data collection. All measurements were followed for ~5−6 times of the half-life of the reaction.

Results

Syntheses. Compounds synthesized in this study are shown in Chart 1. Dioxo-Mo^{VI} complexes, Tp*MoO$_2$(S-*p*-RC$_6$H$_4$) (**1**) were synthesized following literature procedure[49] by reacting Tp*MoO$_2$Cl with *para*-substituted thiophenols in the presence of Et_3N in CH_2Cl_2. Reactions were found to be complete within 2−6 h as evidenced by thin layer chromatography, and the target compounds were purified by chromatography on silica columns using toluene (for R = OMe, Me, H, Cl, and CF_3) or a mixture of toluene and acetonitrile (for R = NHCOMe and NO_2) as the eluent. All dioxo-Mo^{VI} complexes were obtained as brown solids and found to be stable in air in the solid state.

The $OPMe_3$ coordinated monooxo-Mo^{IV} intermediate complexes Tp*MoO(S-p-RC$_6$H$_4$)(OPMe$_3$) (**2**) were synthesized by an incomplete transfer of an oxygen atom between dioxo complexes and PMe_3 in non-coordinating solvents such as benzene or toluene under ambient conditions. In most cases, the color of the reaction has changed from brown to green within 30−40 min after addition of PMe_3. The phosphoryl intermediate complexes were purified by precipitation from the reaction mixture by adding excess hexane. The same reaction with PMe_3 and **1d** or **1h** did not yield pure phosphoryl complexes in benzene or in toluene.

NMR Spectra. All molybdenum complexes described in here are diamagnetic and are amenable to NMR spectroscopy (Supporting Information, Tables S1, S2, and S3). The ^{1}H NMR spectra revealed C_s symmetry in **1** and C_1 symmetry for **2**, which is consistent with the reported Tp*MoO$_2$X and Tp*MoOX(OPMe$_3$) complexes.[40,45,50,51] The ^{31}P NMR spectra of **2** in benzene displayed a resonance at ~ 62.0 (±1) ppm for the coordinated $OPMe_3$, which was deshielded by about 26 ppm relative to the free $OPMe_3$ (36.2 ppm). ^{31}P-chemical shifts were found to be insensitive to the substitution at the para-position of the thiophenolate ring. Solution of **2** in

(47) *teXsan: Crystal Structure Analysis Package*; Molecular Structure Corporation: The Woodlands, TX, 1985, 1992

(48) Betteridge, P. W.; Carruthers, J. R.; Cooper, R. I.; Prout, K.; Watkin, D. J. *J. Appl. Crystallogr.* **2003**, *36*, 1487.

(49) Xiao, Z.; Bruck, M. A.; Doyle, C.; Enemark, J. H.; Grittini, C.; Gable, R. W.; Wedd, A. G.; Young, C. G. *Inorg. Chem.* **1995**, *34*, 5950.

(50) Xiao, Z. G.; Bruck, M. A.; Doyle, C.; Enemark, J. H.; Grittini, C.; Gable, R. W.; Wedd, A. G.; Young, C. G. *Inorg. Chem.* **1996**, *35*, 5752.

(51) Nemykin, V. N.; Basu, P. *Dalton Trans.* **2004**, 1928.

acetonitrile exhibited a developing signal for free $OPMe_3$ at 36.2 ppm, indicating dissociation of the coordinated $OPMe_3$ in the acetonitrile.

The ^1H NMR spectra of Tp*MoO(S-*p*-$OMeC_6H_4$)($OPMe_3$) were investigated in four different solvents (Supporting Information, Table S3), which shows solvent dependent chemical shifts. In polar solvents, for example, acetonitrile and acetone, pyrazole methyl protons resonate between 1.8 and 2.6 ppm, while in non-polar aromatic solvents, for example, toluene and benzene, they shift to higher fields (2.20−2.8 ppm). Interestingly, larger solvent effect was observed for $OPMe_3$ (∼0.7 ppm) and OMe (∼0.5 ppm) groups but only a small change in the pyrazole C−H and thiophenol signals. The effect of temperature has also been studied in acetonitrile from −40 °C to +35 °C but no significant changes were observed.

Infrared Spectra. Tables S1 and S2 (Supporting Information) also list selected infrared spectral data. The dioxo complexes exhibit two strong bands for a *cis*-MoO_2 unit in **1** at ∼930 cm^{-1} and 900 cm^{-1} assigned to the symmetric and asymmetric vibrational modes, respectively. Other characteristic bands include a sharp B−H stretch at 2545 cm^{-1} for **1** which shifted to ∼20 cm^{-1} toward lower frequencies in **2**. For **2**, sharp bands were observed at ∼945 cm^{-1} and ∼1120 cm^{-1} due to the Mo^{IV}=O vibration and P=O vibrations, respectively.

Electronic Spectra. UV−visible spectra of **1** and **2** were recorded in methylene chloride and in acetonitrile, respectively, and the data are tabulated in Tables S1 and S2 (Supporting Information). For **1**, a band around 415 nm ($\varepsilon > 1000$ $M^{-1}cm^{-1}$) due to the S → Mo charge transfer band was observed. A hypsochromic (or blue) shift from **1a** (424 nm) to **1h** (404 nm) was observed because of the substituent present at the *para*-position of the thiophenolato ligand. An intense transition around 260 nm ($\varepsilon > 13000$ $M^{-1}cm^{-1}$) can be assigned as intraligand excitation. In **1h** this band moved to 335 nm probably because of the electron withdrawing NO_2 substituent. The energy of this low-energy band in **1** at ∼500 nm varies linearly with the Hammett constants (σ_p) of the substituents (σ_p: OMe, −0.27; Me, −0.17; SMe, 0.0; NHCOMe, 0.0; H, 0.0; Cl, +0.23; CF_3, +0.54; NO_2, +0.78)[52] following eq 2. The linear relation ($R^2 = 0.88$) indicates that the electronic contribution from the thiophenol ring

$$E(\mathrm{cm}^{-1}) = 18836\ (\pm 113) + 1428\ (\pm 269) \times \sigma_p \quad (2)$$

makes significant contribution to the transition energy.

The Mo(IV) phosphoryl complexes (**2a**−**2g**) exhibit a low energy low intensity d-d transition at ∼760 nm which is consistent with other similar phosphoryl complexes.[45] This band has been tentatively assigned as due to the $d_{xy} \rightarrow d_{xz,yz}$ transition. A band around ∼410 nm can be assigned as the $S(p_\pi) \rightarrow Mo(d_{xz})$ charge transfer transition with possible contributions from $d_{xy} \rightarrow d_{x2\text{-}y2}$ excitation expected for this energy region.[45,53] Interestingly, this band ($\varepsilon \sim 360-680$ $M^{-1}cm^{-1}$) exhibits lower intensity than a typical charge transfer transition, probably because of the unfavorable orientation of the S (p_π) orbitals with respect to the Mo(d_{xz}) atomic orbital, and similar geometry dependence is known for other molybdenum complexes with at least one arylthiol ligand.[54] The energy of this transition does not linearly correlate with the Hammett constants on the thiophenol ring.

Crystallography. Three-dimensional molecular structures were determined by single crystal X-ray crystallography (Figures S1 and S2, Supporting Information), and representative structures are shown in Figure 1. The crystallographic parameters are listed in Tables 1 and 2, and the metric parameters are placed in Tables S4−S5 (Supporting Information). The ligands are arranged in a distorted-octahedral geometry about the metal with a local C_s geometry in **1** and C_1 geometry in **2** at the metal center. The coordination sphere of the dioxo-complexes is composed of the facially coordinating tridentate Tp* ligand, a pair of terminal oxo ligands, and the sulfur of the thiophenolato ligands. Similarly, in the coordination sphere of the monooxo-complexes, the three monodentate ligands (=O, S-*p*-RC_6H_4, —$OPMe_3$) are constrained by the *facial* stereochemistry of the Tp* ligand.

The metric parameters of dioxo-Mo^{VI} complexes were found to be similar to those observed for **1e**.[41] The Mo=O bond distances lie in the range from 1.670(11)−1.710(2) Å, in the region of a typical oxo-Mo^{VI} bond. The Mo−S bond distances, as expected, range from 2.408(4)−2.419(2) Å. There is no systematic variation in the Mo−S bond distance as a function of the *para*-substituents on the thiophenolato ligand. The S−C(41) bond distances (1.767(17)−1.806(14) Å) are also consistent with the reported values for thiophenol and disulfides.[55] A strong trans influence from the oxo-ligands lengthened the Mo−N bond (i.e., Mo−N(11) and Mo−N(21): 2.278(9)−2.349(6) Å) compared to the Mo−N(31) bond (2.156(6)−2.183(11) Å). The O(1)=Mo=O(2) bond angles (103.2(2)−104.4(5)°) are higher than the octahedral bond angle (90°) as are the O=Mo−S bond angles presumably because of repulsions between the π-electrons of the donor atoms. It is interesting to note that O(1)=Mo−S and O(2)=Mo−S bond angles are slightly different, which makes the two terminal oxo-groups inequivalent. The inequivalency of the two terminal oxo-groups in a dioxo-Mo center was explained on the basis of the anisotropic covalent interaction of thiophenolato ligand.[56] The covalent interaction is modulated by the O=Mo−S−C(41) dihedral and the O=Mo−S bond angles (Supporting Information, Table S4). The two dihedral angles O(1)=Mo−S−C(41) and O(2)=Mo−S−C(41) are distinctly different which corroborates the inequivalency of the two oxo groups. In these structures the position of the Tp* ligand is constant, but the orientation of the thiophenol ring along the S−C bond is found to be different. This change in the orientation is understood with the help of Mo−S−C(41)−C(42/46) torsion angle and Mo−S−C(41) bond angles. Different torsion angles in compounds with

(52) Hansch, K.; Leo, A.; Taft, R. W. *Chem. Rev.* **1991**, *91*, 165.
(53) Nemykin, V. N.; Basu, P. *Inorg. Chem.* **2003**, *42*, 4046.
(54) McNaughton, R. L.; Mondal, S.; Nemykin, V. N.; Basu, P.; Kirk, M. L. *Inorg. Chem.* **2005**, *44*, 8216.
(55) Sengar, R. S.; Nemykin, V. N.; Basu, P. *New J. Chem.* **2003**, *27*, 1115.
(56) Helton, M. E.; Pacheco, A.; McMaster, J.; Enemark, J. H.; Kirk, M. L. *J. Inorg. Biochem.* **2000**, *80*, 227.

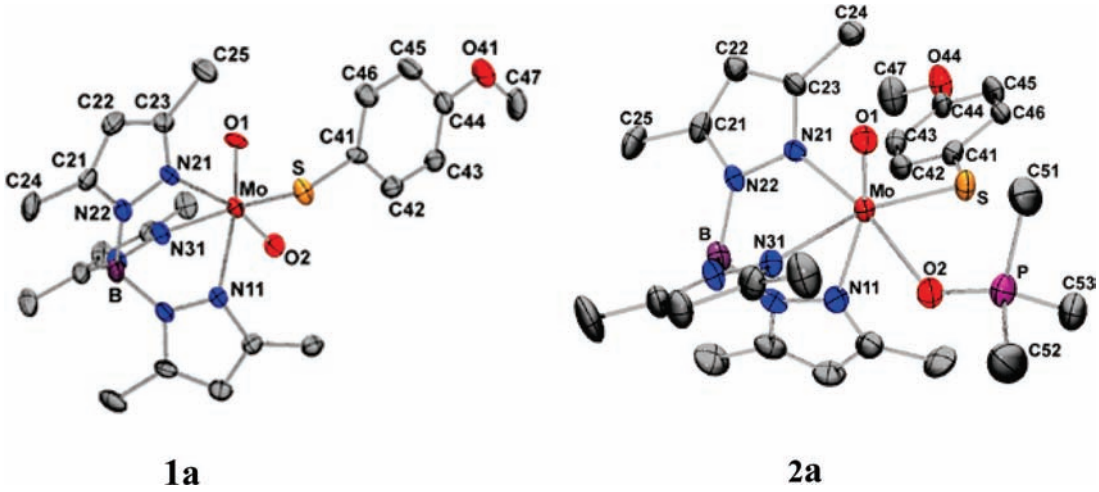

Figure 1. ORTEP diagrams of **1a** and **2a** shown at 40% probability levels. Hydrogen atoms have been omitted for clarity. These two structures are shown as representative examples, complete ORTEP structures are placed in the Supporting Information.

Table 1. Crystallographic Data for Tp*MoO_2(S-*p*-RC_6H_4) (**1**)

	1a	**1b**	**1d**	**1f**	**1h**
formula	$C_{22}H_{29}B_1Mo_1N_6O_3S_1$	$C_{22}H_{29}B_1Mo_1N_6O_2S_1$	$C_{30}H_{38}B_1Mo_1N_7O_3S_1$	$C_{24}H_{29}B_1Mo_1N_6O_2S_1Cl_1$	$C_{21}H_{26}B_1Mo_1N_7O_4S_1$
formula mass	564.33	548.30	683.49	607.80	579.30
crystal system	triclinic	monoclinic	triclinic	triclinic	monoclinic
space group	$P\bar{1}$	$P2_1/c$	$P\bar{1}$	$P\bar{1}$	$P2_1/c$
a(Å)	10.993(4)	18.772(13)	12.4168(17)	10.378 (4)	11.898(2)
b(Å)	12.151(4)	8.136(6)	13.7887(18)	13.601 (4)	16.203(3)
c(Å)	9.892(2)	18.494(13)	10.5214(15)	10.352 (2)	12.887(3)
α(deg)	96.21(2)		96.732(11)	107.346 (18)	
β(deg)	104.05(2)	117.723(9)	113.826(10)	97.29 (3)	91.55(3)
γ(deg)	88.57(3)		81.333(11)	89.52 (3)	
V(Å^3)	1274.2(7)	2500.0(3)	1625.9(4)	1382.8 (7)	2483.5(8)
Z	2	4	2	2	4
d_{calc} (mg/m^3)	1.471	1.457	1.396	1.460	1.549
data collected	3362	1659	6782	2639	2409
$R(F^2)$	0.067	0.053	0.033	0.086	0.114
$wR(F^2)$	0.114	0.218	0.065	0.143	0.345

Table 2. Crystallographic Data for Tp*MoO(S-*p*-RC_6H_4)($OPMe_3$) (**2**)

	2a	**2f**	**2g**
formula	$C_{31}H_{44}B_1Mo_1N_6O_3S_1P_1$	$C_{30}H_{41}B_1Mo_1N_6O_2S_1P_1Cl_1$	$C_{32}H_{43}B_1Mo_1N_6O_2S_1P_1F_3$
formula mass	718.52	722.94	770.52
crystal system	monoclinic	monoclinic	monoclinic
space group	$P2_1/c$	$P2_1/c$	$C2/c$
a(Å)	11.991 (2)	18.150(4)	28.649(8)
b(Å)	10.675 (2)	11.194(2)	11.032(6)
c(Å)	28.378(6)	18.367(4)	26.998(7)
β(deg)	94.47(3)	106.14(3)	118.046(18)
V(Å^3)	3621.5(13)	3584.6(13)	7531(5)
Z	4	4	8
d_{calc} (mg/m^3)	1.318	1.340	1.359
data collected	4264	4728	5992
$R(F^2)$	0.075	0.054	0.067
$wR(F^2)$	0.155	0.118	0.165

different substituents indicate rotational freedom of the phenyl ring along the C(41)−S bond. The Mo−S−C(41) angle also changed from 101.3(2)° in **1a** to 110.7(6)° in **1h**. Both factors would dictate the orientation of the S π orbitals with respect to the molybdenum orbitals and therefore could influence the Mo−S covalency.

The crystal structure of a representative monooxo-Mo^{IV} phosphoryl complex is shown in Figure 1 and all structures can be found in Figure S2, Supporting Information. The metric parameters are listed in Table S5 (Supporting Information). The Mo=O bond distance (1.665(4)−1.686(5) Å) was found to be typical for such complexes.[37,38,40,41,45,57] In most cases, the Mo=O distance is, however, slightly shorter than that in corresponding dioxo-Mo^{VI} complexes. The Mo−O bond lengths (2.153(6)−2.175(5) Å) are similar to those observed in other O=Mo-OPR_3 complexes.[37,38,40,41,45,57]

(57) Doonan, C. J.; Millar, A. J.; Nielsen, D. J.; Young, C. G. *Inorg. Chem.* **2005**, *44*, 4506.

The O(2)=P bond lengths (1.484(4)−1.519(4) Å) are sufficiently smaller than the O−P single bond found in P_4O_{10} (1.6 Å),[40] indicating the involvement of multiple bonding. Interestingly, O(1)−Mo−O(2) bond angles (98.6(2)−99.8(3)°) are reduced from their dioxo-Mo counterparts and are closer to a typical octahedral value indicating a reduction in the π-electron interactions between two oxygen ligands.

Compared to the dioxo complexes, there is no noticeable change in the Mo−S bond lengths, although the S−C(41) bond length is found to be slightly (ca. 0.01 Å) longer. The Mo−N(n1) (n = 1−3) distances are consistent with the expected values based on the *trans* influence of the coligands, namely, =O > S-*p*-RC_6H_4 > $OPMe_3$. The O(2)−Mo−N(n1) angles approached to the ideal octahedral arrangement (∼90°) for n = 2 and 3 but for n = 1, the values are still obtuse (by ∼ 10−15°). The O(1)−Mo−S angle shows a small increase (∼3°), however, O(2)−Mo−S shows a large decrease of about 15° compared to the dioxo complexes. Unlike the parent dioxo-complexes, superimposition of the structures of the phosphoryl complexes exhibits little variation.

Electrochemistry. The electrochemical behaviors of the dioxo-Mo^{VI} complexes and the monooxo-Mo^{IV} phosphoryl complexes were investigated by cyclic voltammetry, the redox potentials are summarized in Table 3, and representative voltammograms are shown in Figure 2. With the exception of **1h**, all dioxo-complexes exhibited a well-defined one-electron redox couple due to Mo(VI/V) reduction similar to those reported earlier.[49,58] The redox couple in complex **1h** was irreversible, the precise reason for the irreversibility is currently not clear, although we assume the redox noninnocent nature of the *p*-NO_2 substituent is playing a role.

The phosphoryl complexes also exhibit a reversible one-electron oxidation couple due to the Mo^V/Mo^{IV} couple. The linear dependence of the peak currents with the square root of the scan rate and the ratio of the cathodic-to-anodic peak current close to unity indicate a diffusion controlled process. The peak-to-peak separation values are found to be close to what is expected for a typical one electron redox process. The reversible nature of the voltammograms indicates that the compounds are electrochemically stable. Displacement of phosphine oxide by a solvent (MeCN in this case) generate compound **3** which exhibits a more positive reduction potential (Figure 2). This spontaneous transformation has been discussed in detail for compound **2e**.[41] At room temperature the rate of transformation of **2e** to **3e** was determined from electrochemistry to be 5.6×10^{-4} sec^{-1}, which is consistent with that determined by optical spectroscopy. The reduction potentials of the phosphoryl complexes as well as the parent dioxo-Mo^{VI} complexes follow a linear relation with the Hammett constant of the *para*-substituent at the thiophenol (Figure 2, right panel). The effect of substituents on the reduction potential is discussed later.

Kinetics. We have reported that phosphoryl complexes undergo solvolysis reaction in coordinating solvents such as acetonitrile, as evidenced by a change in color of the solution.[32,41] Consistent with this, freshly prepared acetonitrile solution of pure **2a** slowly changes from green to cyan color, which has been monitored by optical spectroscopy (Figure 3b). At 22 °C, two distinct isosbestic points (at 398 nm and at 670 nm) were observed in this case, indicating a clean transformation at this temperature.

Table 3. Redox Potentials of **1** and **2** in MeCN at Room Temperature[a]

complexes	$E_{1/2}$(V)	ΔE_p(mV)
1a	−1.170	126
1b	−1.130	88
1c	−1.120	68
1d	−1.150	79
1e	−1.110	120
1f	−1.070	65
1g	−1.030	134
2a	−0.550	81
2b	−0.540	68
2c	−0.510	68
2e	−0.530	69
2f	−0.490	66
2g	−0.460	78

[a] Potentials are expressed with respect to Fc^+/Fc couple.

The brown color acetonitrile solution of the dioxo-complexes changed to green when reacted with PMe_3 and finally to cyan. Figure 3a shows the time dependent optical spectra of acetonitrile solution of **1a** when reacted with PMe_3 at 10 °C. In this case, no distinct isosbestic point was observed. The two step process is evident as the LMCT transition at 414 nm decreases in two steps-first a quick decrease (∼3−5 min depending upon the amount of PMe_3 and the temperature), followed by a slower (∼40−60 min) process. At the same time a low energy band due to the d-d transition at ∼750 nm grew at a comparable rate to that of the decay of the 414 nm band. As mentioned, the optical spectra of the acetonitrile solution of **2a** exhibit distinct isosbestic points at 398 and 670 nm; however, no such isosbestic point was observed for the reaction of **1a** with PMe_3 (inset of Figure 3a). Assuming no other reactions contributing significantly to the overall spectral profile, any spectral change at 398 nm in the reaction of **1a** with PMe_3 represents the formation of **2a**. Thus, single wavelength assay were conducted at 398 nm for the formation of the phosphoryl complex **2a**. In the case of decomposition of **2a**, maximum change in absorbance was observed at 414 nm and therefore assays were performed at that wavelength. The activation parameters were computed from temperature dependent rate constants (Table 4).

The reaction of **1a** with PMe_3 was followed at ∼398 nm under pseudo first order condition from which the second order rate constants were calculated (Supporting Information, Table S6). Similarly reactions of PMe_3 with other dioxo-Mo^{VI} complexes were monitored at an appropriate wavelength (Supporting Information, Table S7), and the activation parameters were determined from temperature dependent rate constants (Table 4). Both steps of the reaction of **1** with PMe_3 could be followed spectrophotometrically as time constants of the two steps are different.

Discussion

A series of new dioxo-Mo(VI) complexes coordinated by a substituted thiophenol have been synthesized and characterized.

(58) Millar, A. J.; Doonan, C. J.; Laughlin, L. J.; Tiekink, E. R. T.; Young, C. G. *Inorg. Chim. Acta* **2002**, *337*, 393.

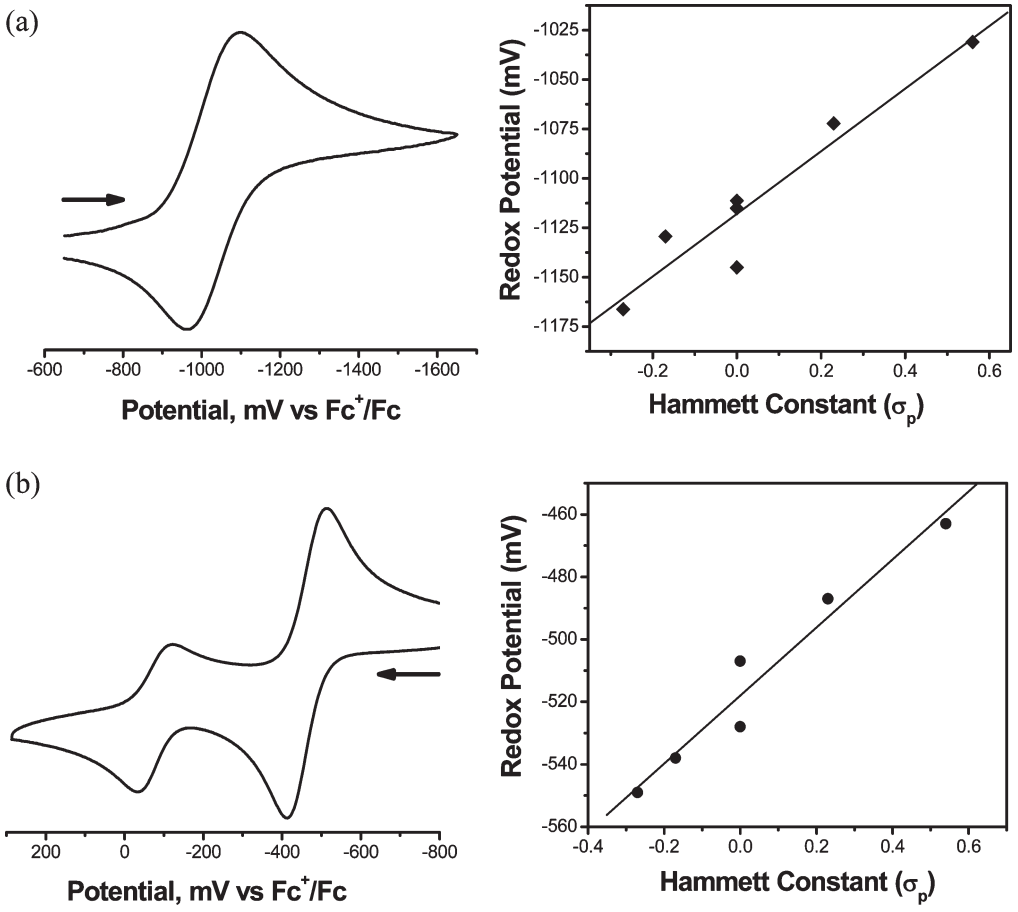

Figure 2. Cyclic voltammograms of a representative dioxo-Mo^{VI} complex, Tp*MoO_2(S-*p*-$CF_3C_6H_4$), (**1g**) (**a**, left panel, top), and a representative phosphoryl-Mo^{IV} complex, Tp*MoO (S-*p*-$CF_3C_6H_4$)($OPMe_3$), (**2g**) (**b**, left panel, bottom), in MeCN at a scan rate of 100 mV/s. An extra redox response at around 100 mV found in **2g** is due to the formation of solvent coordinated complex; note that this trace was recorded after 15 minutes of dissolution of **2g**. Right panels of **a** and **b** show the linear dependence of redox potentials with σ_p.

The synthetic route leading to these compounds is already established, and the successful syntheses of the molecules described in here underscore the robustness of the methodology.[41,49] The Mo═O vibrations (~923 and ~893 cm^{-1}) do not exhibit a large variation; however, the lower energy band near 500 nm in their optical spectra differ by 37 nm (1420 cm^{-1}) from electron donating OMe substituent in **1a** to electron withdrawing NO_2 group in **1h**. The protons of the thiophenol ring are appropriately shifted upfield (for electron donating substituent) or downfield (for electron withdrawing substituent) in their ^1H NMR spectra; however, little or no change was observed in the chemical shift of the pyrazole ring. This indicates that the remote substitution at the thiophenol ring does not influence the electronic environment of the Tp*.

Molybdenum(IV) phosphoryl intermediate complexes were synthesized by incomplete oxo-transfer reaction with PMe_3 as an oxo-abstractor. However, compounds **1d** and **1h** are sparingly soluble in benzene or toluene, and the reactions with PMe_3 did not yield the target phosphoryl complex; instead red colored solutions resulted that are reminiscent of μ-oxo-dimeric compounds. Like **1**, no or little change in the Mo═O vibration (~947 cm^{-1}) or P═O (~1114 cm^{-1}) has been observed. The ^{31}P NMR was found to be invariant, while the low energy band near ~778 nm in the optical spectra showed a modest variation (by ~15 nm, 287 cm^{-1}). Thus, the substituent effect on the equatorial thiophenol ring is more prominent in the dioxo-Mo^{VI} complexes.

Structural Changes. The metric parameters of the dioxo-Mo^{VI} and phosphoryl intermediate complexes are similar to those reported earlier, which includes the Mo═O, Mo−N, and Mo−S bond lengths.[37,38,40,41,45] The metal centers in both dioxo-Mo^{VI} and monooxo-Mo^{IV} complexes are distorted octahedral with strong *trans*-effect from the Mo═O bond, and in the phosphoryl complexes, the P═O bond exhibits a double bond character. Figure 4 shows the superimposition of the structure of crystallographically characterized dioxo-complexes which highlights different orientations of the thiophenol ring. Compared to the dioxo-Mo^{VI} complexes, in general there is an increase in the Mo−S−C angle in the phosphoryl complexes, as well as a change in the orientation of the thiophenol ring. A significant structural reorientation of the thiophenol ring in Tp*MoO(SC_6H_5)($OPMe_3$) compared to Tp*MoO_2(SC_6H_5) has been observed recently.[41] A very similar structural reorganization was observed in the reaction pairs Tp*MoO_2(S-*p*-$OMeC_6H_4$)/ Tp*MoO (S-*p*-$OMeC_6H_4$)($OPMe_3$) and Tp*MoO_2(S-*p*-ClC_6H_4)/ Tp*MoO(S-*p*-ClC_6H_4)($OPMe_3$) (Figure 5). These structural changes are observable with a small tertiary phosphine (PMe_3) but was not observed with a larger phosphine, that is, PEt_3 in a similar system, where a phenol takes the position of the thiophenol.[57] While the origin of this structural reorganization is yet to be understood clearly, superimposition of the structures of

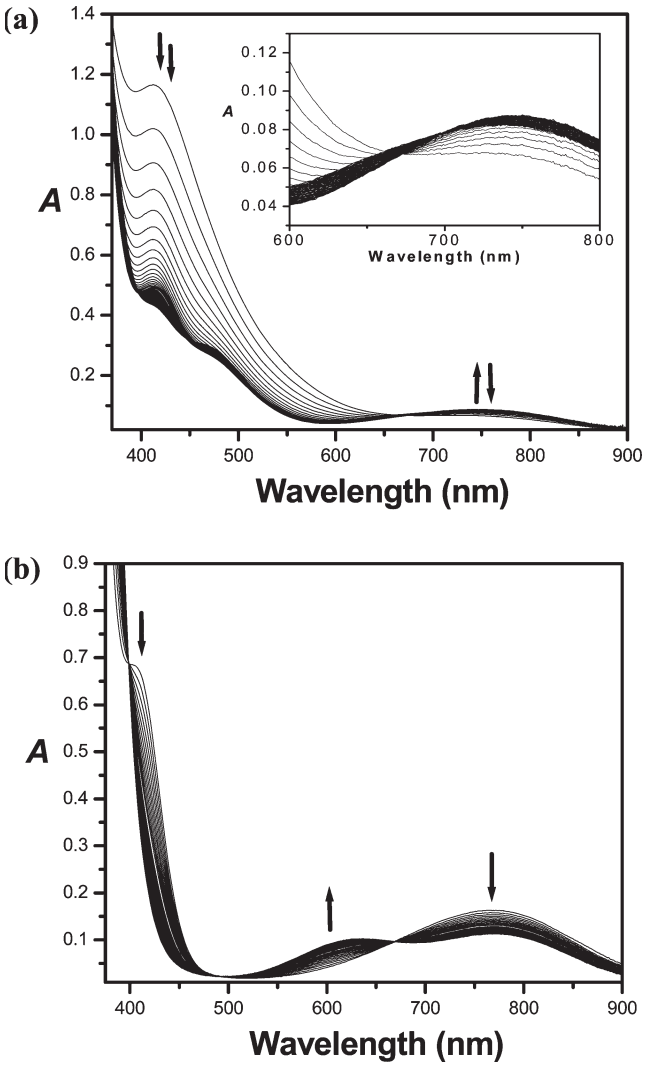

Figure 3. UV−visible spectral changes in MeCN. (a) During the oxidation of PMe_3 by **1a** at 10 °C, [**1a**]:[PMe_3] = 1:20 ([**1a**] = 0.35 mM); time interval between each scan = 1.4 min. The inset shows the absence of an isosbestic point. (b) Decomposition of **2a** at 22 °C, [**2a**] = 2.53 mM, time interval between each scan = 5.5 min.

Tp*MoO_2(S-*p*-$OMeC_6H_4$)/Tp*MoO(S-*p*-$OMeC_6H_4$)($OPMe_3$) pair indicates that a twist of the thiophenol ring away from the point of attack by the phosphine, rotating the thiophenolato ring clockwise along the Mo···B vector. Such a conformational change would influence the metal−sulfur interaction and covalency as proposed in Cu−S(cysteine) and Mo−S(cysteine) interactions in native systems.[59,60] The large variations in the structural features in the thiophenolato ligand show the involvement of the first coordination sphere as well as the second coordination sphere in the OAT reaction, which has been proposed to play an important role in the redox and OAT processes of analogue and natural oxotransferase systems.[60,61] While the aliphatic thiol, for example, cysteine, offers more structural flexibility, aromatic thiols provides more electron conjugation.

Substituent Effects on the Redox Potentials. In an octahedral oxo-Mo^V center, the redox orbital is the half-filled d_{xy} orbital; reduction to oxo-Mo^{IV} would involve further addition of an electron into this orbital, and oxidation would involve loss of an electron from this orbital. A number of factors influence the redox potency of oxo-Mo^V centers such as the chelate ring size and torsion angle, as well as the electronic properties of remote substituents.[62−65] In contrast to the Mo^V complexes, the redox properties of Mo^{IV} or Mo^{VI} centers have received less attention, in part because of the lack of reversible redox couples in dioxo-Mo^{VI} complexes. Dioxo-Mo^{VI} complexes of pyrazolyl borate such as **1**, however, exhibit reversible $Mo^{VI/V}$ reduction couple.[49] The phosphoryl complexes (**2**) also exhibit a reversible one-electron $Mo^{IV/V}$ oxidative couple. The $Mo^{VI/V}$ reduction potential in **1** appears at a more negative potential than the $Mo^{V/IV}$ couple in **2**. The $Mo^{VI/V}$ reducion potential span from −1166 mV in **1a** to −1031 mV in **1g**, a difference of 135 mV, whereas the Mo(V/IV) potential span from −549 mV in **2a** to −463 mV in **2g**, a difference of 86 mV. The reduction potentials for both couples vary as a function of substituents at the *para* position of the thiophenolato ring. In **1**, electron withdrawing groups make the complex easier to reduce and in **2**, electron-withdrawing groups make the oxidation process difficult. The sensitivity of reduction potentials is understood from the Hammett correlation. The reduction potentials vary linearly (Figure 2) with the Hammett constants (σ_p) of the substituents at the *para* position of the thiophenol ring (eqs 3 and 4 are for **1** and **2**, respectively):

$$E_{1/2}(\mathrm{mV}) = 158\ (\pm 23)\times \sigma_p - 1118\ (\pm 6)\ (R^2 = 0.91) \quad (3)$$

$$E_{1/2}(\mathrm{mV}) = 109\ (\pm 13)\times \sigma_p - 518\ (\pm 4)\ (R^2 = 0.95) \quad (4)$$

The slope of the lines indicates the sensitivity of the process on the substituent. Clearly, the dioxo-Mo^{VI} complexes are more sensitive to the substituents compared to the oxo-Mo^{IV} phosphoryl complexes, which indicates stronger π interaction of the sulfur orbitals with the Mo d-orbitals. This effect is also manifested in the smaller Mo−S−C angle. Interestingly, the redox potentials in oxo-Mo^V centers in Tp*MoOCl(O-*p*-RC_6H_4) and Tp*MoO(O-*p*-$RC_6H_4)_2$ complexes are more sensitive to the substitutents.[62] While these complexes are compositionally and structurally different, a metal ligand distance (d(Mo−S) > d(Mo−O)) may lead to a higher sensitivity.

Mechanism of OAT Reaction. The first step in the OAT reaction from a dioxo-Mo^{VI} center to a tertiary phosphine involves nucleophilic attack on the Mo=O

(59) Gamelin, D. R.; Williams, K. R.; LaCroix, L. B.; Houser, R. P.; Tolman, W. B.; Mulder, T. C.; de Vries, S.; Hedman, B.; Hodgson, K. O.; Solomon, E. I. *J. Am. Chem. Soc.* **1997**, *119*, 613.
(60) Peariso, K.; Helton, M. E.; Duesler, E. N.; Shadle, S. E.; Kirk, M. L. *Inorg. Chem.* **2007**, *46*, 1259.
(61) Kirk, M. L.; Peariso, K. *Polyhedron* **2004**, *23*, 499.
(62) Graff, J. N.; McElhaney, A. E.; Basu, P.; Gruhn, N. E.; Chang, C.-S. J.; Enemark, J. H. *Inorg. Chem.* **2002**, *41*, 2642.
(63) Chang, C. S. J.; Pecci, T. J.; Carducci, M. D.; Enemark, J. H. *Inorg. Chem.* **1993**, *32*, 4106.
(64) Chang, C. S. J.; Enemark, J. H. *Inorg. Chem.* **1991**, *30*, 683.
(65) Chang, C. S. J.; Collison, D.; Mabbs, F. E.; Enemark, J. H. *Inorg. Chem.* **1990**, *29*, 2261.

Table 4. Activation Parameters for the Formation of **2** and **3**

starting complex	λ_{abs}[a] (nm)	$E_a^{\ddagger}$ (kJ·mol^{-1})	ln A	$\Delta H^{\ddagger}$ (kJ·mol^{-1})	$\Delta S^{\ddagger}$ (J mol^{-1} K^{-1})	$\Delta G^{\ddagger}_{297}$ kJ·mol^{-1}
		Tp*MoO$_2$(S-*p*-RC$_6$H$_4$) + OPMe$_3$ → Tp*MoO(S-*p*-RC$_6$H$_4$)(OPMe$_3$)				
1a	398	51.7(±4.1)	11.9(±1.7)	49.3(±4.1)	−154.0(±14.2)	95.0
1b	395	49.7(±8.7)	12.0(±3.6)	47.3(±8.7)	−153.3(±30.1)	92.8
1e	393	41.2(±1.3)	9.0(±0.6)	38.8(±1.3)	−178.4(±4.7)	91.8
1f	396	48.3(±1.0)	12.1(±0.4)	45.9(±1.0)	−152.6(±3.6)	91.2
1g	398	36.4(±7.5)	8.3(±3.2)	34.0(±7.5)	−184.3(±26.1)	88.7
		Tp*MoO(S-*p*-RC$_6$H$_4$)(OPMe$_3$) + MeCN → Tp*MoO(S-*p*-RC$_6$H$_4$)(MeCN) + OPMe$_3$				
2a	414	64.9(±2.2)	18.3(±1.0)	62.5(±2.2)	−101.3(±7.5)	92.7
2b	414	69.5(±2.5)	20.2(±1.0)	66.9(±2.5)	−85.7(±8.3)	92.4
2c	414	68.3(±1.0)	19.8(±0.4)	65.8(±1.0)	−88.3(±8.8)	92.0
2e	412	70.4(±1.0)	20.6(±0.4)	67.8(±1.0)	−82.5(±3.3)	92.3
2f	418	67.6(±0.1)	19.6(±0.1)	65.1(±0.2)	−90.0(±0.5)	91.8
2g	424	65.0(±3.3)	18.8(±1.3)	62.6(±3.3)	−96.8(±11.0)	91.4

[a] Wavelength at which the assay was conducted.

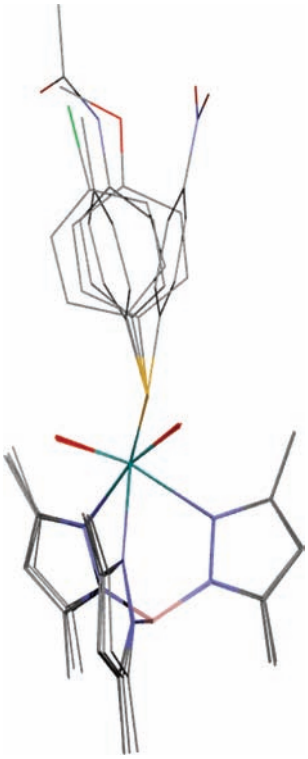

Figure 4. Superimposition of the crystal structures (line diagrams) of Tp*MoO$_2$(S-*p*-RC$_6$H$_4$).

π*-orbital by the phosphorus lone pair, with simultaneous nucleophilic attack on the P−C σ* orbital by the terminal oxo-group. This results in a hypervalent character of the phosphorus at the transition state and ultimately two-electron reduced phosphoryl intermediate complex.[32] The next step of reaction is a solvolysis reaction where the phosphine oxide is replaced by a solvent molecule. Variable temperature kinetic measurements allowed determining the activation parameters for both steps (Table 4).

For the first step, a large negative values of the entropy of activation ($\Delta S^{\ddagger}$: −152.6 to −184.3 J·mol^{-1}·K^{-1}) suggest an associative transition state. A relatively small activation enthalpy ($\Delta H^{\ddagger}$: 34.0 to 49.3 kJ·mol^{-1}) is associated with this process similar to that observed for other alkyl phosphine (e.g., PEt$_3$) suggests the formation of a strong P=O bond at the expense of a Mo=O bond.[32]

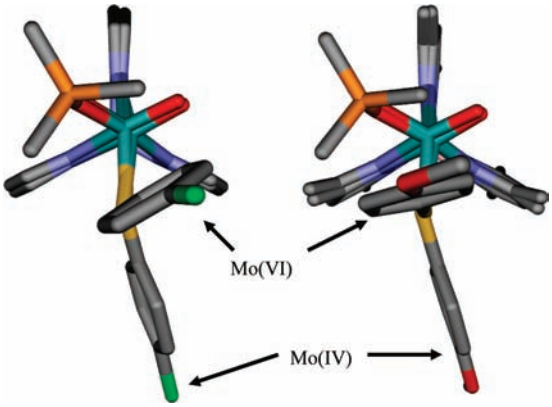

Figure 5. Superimposition of the crystal structures (tube diagrams) of Tp*Mo^{VI}O$_2$(S-*p*-ClC$_6$H$_4$)/Tp*Mo^{IV}O(S-*p*-ClC$_6$H$_4$)(OPMe$_3$) in left and Tp*Mo^{VI}O$_2$(S-*p*-OMeC$_6$H$_4$)/Tp*Mo^{IV}O(S-*p*-OMeC$_6$H$_4$)(OPMe$_3$). Note the rotation of the thiophenol ring away from the coordinated phosphine oxide.

Considering the substrate being the same (PMe$_3$), the difference in the enthalpy of activation likely to reflect a difference in the nucleophilicity as a function of substituent. Overall, the free energy of activation ($\Delta G^{\ddagger}$) showed a small change of ~6.3 kJ·mol^{-1} depending on the substituent at the *para*-position of the thiophenolato ligand.

The substituent effect on the rate of formation of the phosphoryl intermediate complex **2** showed a linear

$$\log(k^{I}_{R}/k^{I}_{H}) = \rho\sigma_p = 0.93\ (\pm 0.29)\sigma_p \qquad (5)$$

dependence of rate constants on the Hammett constant of the substituent, eq 5. The normalized rate constant (k^{I}_{R}/k^{I}_{H}; where k^{I}_{R} represents the rate of the formation of phosphoryl intermediates with substituent R and k^{I}_{H} represents the same reaction with unsubstituted thiophenol) increases with electron-withdrawing groups while it decreases with electron-releasing groups. The linearity (with R^2 = 0.85) indicates that reaction with different substituents follow a similar mechanism. The slope of the plot (ρ) is 0.93 which suggest a strong dependence of the reaction rate.[66,67]

(66) Arias, J.; Newlands, C. R.; Abu-Omar, M. M. *Inorg. Chem.* **2001**, *40*, 2185.
(67) Seymore, S. B.; Brown, S. N. *Inorg. Chem.* **2000**, *39*, 325.

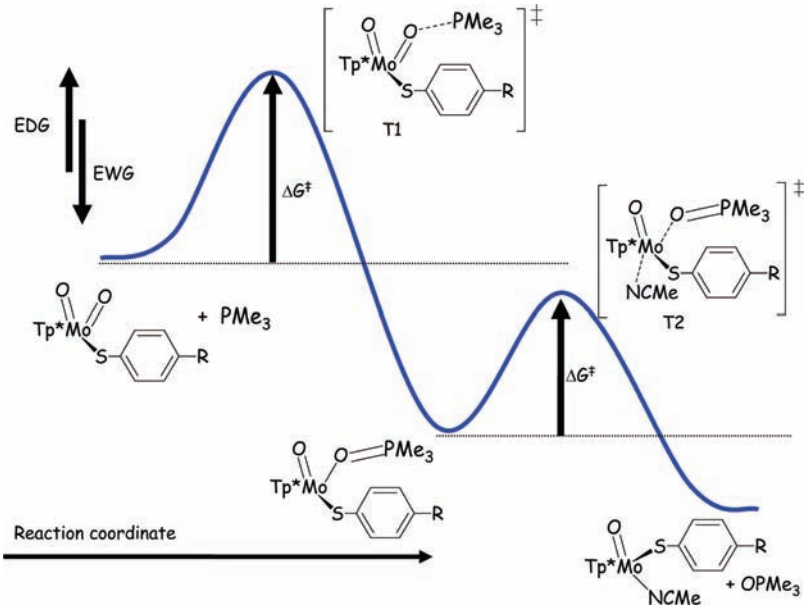

Figure 6. Schematic representation of the OAT reaction of **1** showing the effect of remote substitution.

This observation is consistent with the nucleophilic nature of the phosphine attack where electron-withdrawing groups on dioxo-Mo^{VI} center would decrease the electron density of the oxo-group and therefore making it more susceptible for the nucleophilic attack by the phosphine.

Under the mechanistic proposal, the binding and formation of the phosphine oxide is concomitant with the electron transfer to the metal center. While there is no reliable way to determine the redox potential of this activated complex accurately, the parent compound exhibits a reversible one-electron redox couple, which provides the ground state reduction potential. This ground state reduction potential is indicative of the intrinsic reducibility of the metal center and thus can be correlated with the rate of the reaction. Thus, a plot of the log (k^{I}_{R}/k^{I}_{H}) (where R = OMe, H, Cl, and CF_3) versus difference in the reduction potential $(E_R - E_H)$ provides a linear relation ($R^2 = 0.93$) indicating a similar process is operating in all cases (eq 6). Under the reaction conditions, the linearity then suggests that the reduction of the

$$\log(k^{I}_{R}/k^{I}_{H}) = 0.139\ (\pm 0.022)(E_R - E_H) + 0.007\ (\pm 0.007) \qquad (6)$$

metal center is concomitant with the formation of the phosphoryl intermediate. Interestingly, this finding is inherently different from that reported for the tungsten dithiolene complexes where lack of a correlation with the redox potential with the reaction rate, in part, led to the proposal of a two step model for the overall reaction.[25] In the tungsten system, the metal center acts as an oxo-acceptor while in the present case the metal center acts as an oxo-donor.

The next step in the reaction sequence is the coordination of solvent molecule replacing the coordinated phosphine oxide. In coordinating solvent such as acetonitrile, the reaction proceeds as a first order process depending only on the complex. For this step, a fairly large negative entropy of activation ($\Delta S^{\ddagger}$, −82.5 to −101.3 J/mol.K) was observed. While the values are smaller than those in the first step, they indicate an associative transition state. Thus, we propose the transition state is a seven-coordinated oxo-Mo^{IV} center where both outgoing $OPMe_3$ and incoming MeCN associated with the metal center. It is instructive to point out that the mechanism is different from that found in our previous study with phenolato complexes where small positive entropy of activation indicated a dissociative interchange mechanism.[32] However, a seven-coordinate transition state was computationally located at a higher energy. We attribute this difference in the mechanism to the difference in the metal ligand bond length (d(Mo−S > d(Mo−O)) and a smaller substrate. Furthermore, in the previous study we used a more bulky pyrazolyl borate ligand (Tp^{iPr}) whereas the present investigation used a smaller pyrazolyl borate (Tp*) ligand, which can also contribute to the mechanistic difference.

The major contributing factor to the free energy of activation is the enthalpy of activation, which varies by 4.3 kJ/mol. But the free energy of activation ($\Delta G^{\ddagger}$) is found to be very small (1.3 kJ/mol), and almost invariant to the substituents. The change in the enthalpy is compensated by the entropic contribution which is reminiscent of the entropy compensation effect.[68] It is interesting to note that in the second step of the reaction, the entropic term ($T\Delta S^{\ddagger}$) contributes only ∼30% to the $\Delta G^{\ddagger}$, whereas in the first step of the reaction the $\Delta G^{\ddagger}$ has a much larger contribution (48%−62%) from the entropic term, even though both steps pass through an associative transition state.

The effect of the substituents on the reaction was further understood through the Hammett relation. The $\log(k^{II}_{R}/k^{II}_{H})$ (where k^{II}_{R} represents the rate of solvolysis reaction with substituent R and k^{II}_{H} represents the same reaction with unsubstituted thiophenol) follows a linear relation with the Hammett constant (eq 7).

$$\log(k^{II}_{R}/k^{II}_{H}) = \rho\sigma_p = 0.28\ (\pm 0.04)\sigma_p \qquad (7)$$

(68) Leung, D. H.; Bergman, R. G.; Raymond, K. N. *J. Am. Chem. Soc.* **2008**, *130*, 2798.

A linear correlation ($R^2 = 0.96$) indicates that all complexes follow a similar mechanism with electron withdrawing group increasing the reaction rate; the use of electrophilic substitution constants (σ_p^+) resulted in a poor correlation. The slope of the line, $\rho \sim 0.28$ indicates negative charge build up, although modestly, and more importantly suggests a nucleophilic ligand substitution reaction.

The free energy of activation of the two steps are very similar (Table 4); $\Delta G^{\ddagger}_{297} \sim 91(\pm 4)$ kJ mol^{-1}). This two-step reaction profile can be depicted pictorially in Figure 6, which shows two transition states T1 and T2 and one intermediate. The first transition state T1 primarily involves a partial bond formation between phosphine and one of the oxo ligand in [MoO_2] unit. The second transition state T2 involves a partial solvent coordination to give a seven coordinated environment, resulting in dissociation of the phosphine oxide and formation of a monooxo-Mo^{IV} solvent coordinated product.

This study shows that electron withdrawing groups (EWGs) and electron donating groups (EDGs) have opposite effects in the electron transfer step, that is, the first step of the reaction: the EDGs increase the $\Delta G^{\ddagger}$ value that decrease the rate of the reaction. In this case, the first step becomes rate limiting. Similarly, EWGs decrease the $\Delta G^{\ddagger}$ value and increase the rate of reaction for the first step which makes the second step rate determining. Because the remote substituents affect the two steps of the reaction differently, it is possible to alter the rate limiting step in the overall reaction even with a single remote substituent. Figure 7 shows the ratio of the rate constant (k^I/k^{II}) at 20 °C which clearly indicates the limiting step. For R = Me, both steps are equally balanced, and with an electron donating group the second step becomes rate limiting, while for electron withdrawing groups the first step becomes rate limiting. In the present case, we have used only one phosphine, PMe_3, and it is important to note that the basicity of the substrate also influences the reaction such that the reaction rate is accelerated with more basic phosphines.[69] It is provocative to suggest that in biological systems hydrogen bonding at the active site can play an important role in poising the electron donation to the metal center. In the case of pterin-containing molybdenum enzymes, another possibility is the distortion of the cofactor either at the dithiolene plane or at pyran ring modulating the electron redistribution. In such cases, the rate limiting step of the overall process can be altered. Thus, the redox potential to be modulated by other means such as the hydrogen bonding which is known to modulate the redox properties of dioxo-Mo^{VI} centers.[70]

A two step reaction profile similar to the one described in here has been proposed for the OAT reaction from an oxygen donor (Me_2SO) to a desoxo-W^{IV} analogue complex [W(OPh)($S_2C_2Me_2$)$_2$].[23] The proposed intermediate complex and nature of the transition states were described from chemical principles and kinetic studies. In our proposed profile, the intermediate complex involved in the OAT reaction has been isolated, thoroughly characterized, and in one case (R = H) the solvent coordinated product has also been structurally characterized.[41] The nature of the transition states have been defined by variable temperature kinetic measurements.

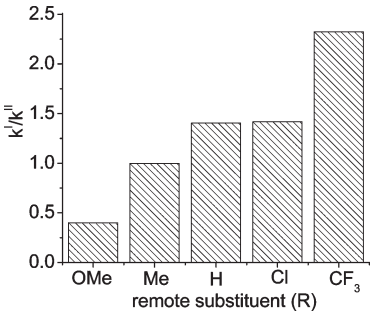

Figure 7. Ratio of rate constants at 20 °C as a function of remote substituent.

Conclusion

This study elucidates the structural and spectroscopic properties of several dioxo-Mo^{VI} complexes coordinated by a single thiophenol ligand, as a function of substituents at the *para* position that are systematically changed. Many of the complexes have similar molecular structures thus exhibiting small structural change among the dioxo-Mo^{VI} complexes. Reaction of the dioxo-Mo^{VI} complexes with PMe_3 led to the formation of monooxo-Mo^{IV} phosphoryl complexes which were also characterized structurally, and spectroscopically.

The kinetics studies depict that the two-step OAT reaction involves associated transition states in both of the steps. Comparison of the rates from both steps shows that the first step is more sensitive toward the substituent effects on the thiophenolato ligand. A similar property has also been extended to the redox potentials of dioxo and intermediate complexes, where redox potentials of dioxo complexes are more sensitive toward substituent effects than the phosphoryl intermediate complexes. Thus, by changing the electronic environment around the metal center one can affect the activation barrier of the first step relative to that of the second step.

Acknowledgment. The authors are grateful to the National Institutes of Health (GM06155502) for financial support.

Supporting Information Available: Crystallographic data in CIF format. Tables of characterization data, metric parameters, and variable temperature rate constants, and ORTEP figures. This material is available free of charge via the Internet at http://pubs.acs.org.

(69) Kail, B. W. Ph.D. dissertation, Duquesne University, Pittsburgh, 2006.

(70) Sengar, R. S.; Miller, J. J.; Basu, P. *Dalton Trans.* **2008**, 2569.